Journal of Natural Gas Science and Engineering 60 (2018) 190–201

Contents lists available at ScienceDirect

Journal of Natural Gas Science and Engineering

journal homepage: www.elsevier.com/locate/jngse

Experimental investigation on the impact of connate water salinity on dispersion coefficient in consolidated rocks cores during Enhanced Gas Recovery by CO_2 injection

Muhammad Kabir Abba[a,*], Athari Al-Othaibi[a], Abubakar Jibrin Abbas[a], Ghasem Ghavami Nasr[a], Abdulkadir Mukhtar[b]

[a] Department of Petroleum and Gas Engineering, University of Salford Manchester, M4 5WT, United Kingdom
[b] Department of Chemical Engineering, Federal University of Technology, PMB 65, Minna, Nigeria

ARTICLE INFO

Keywords:
Enhanced gas recovery
Dispersion coefficient
Connate water salinity
CO_2 sequestration

ABSTRACT

Connate water salinity is a vital property of the reservoir and its influence on the displacement efficiency cannot be overemphasised. Despite the numerous analytical literature on the dispersion behaviour of CO_2 in CH_4 at different parametric conditions, studies have so far been limited to systematic effects of the process while parameters such as connate water salinity of the reservoir has not been given much attention and this could redefine the CO_2–CH_4 interactions in the reservoir. This study aims to experimentally determine the effect of connate water salinity on the dispersion coefficient in consolidated porous media under reservoir conditions. A laboratory core flooding experiment depicting the detailed process of the CO_2–CH_4 displacement using Grey Berea sandstone core sample at a temperature of 50 °C and at a pressure of 1300 psig was carried out to determine the optimum injection rate, from 0.2 to 0.5 ml/min, for the experimentation based on dispersion coefficients and methane recovery in the horizontal orientation. This was established to be 0.3 ml/min. At the same conditions, the effects of connate water saturation of 10% and a salinity of 0 (distilled water), 5, and 10% wt. with a CO_2 injection rate of 0.3 ml/min on the dispersion coefficients was investigated. The results from the core flooding process indicated that the dispersion coefficient decreases with increasing salinity, hence the higher the density of the immobile phase (connate water) the lower the dispersion of CO_2 into CH_4. This is a significant finding given that the inclusion of the connate water and its salinity have an effect on the mixing of the gases in the core sample and should be given importance and included during simulation studies for field scale applications of Enhanced Gas Recovery (EGR). This is the first experimental investigation into the relationship between the connate water salinity and the dispersion coefficient in consolidated porous media.

1. Introduction

As natural gas continues to gain widespread usage as a source of cleaner and efficient fossil fuel, and greenhouse gas emission is attracting environmental consequences, the need for a viable method to enhance and curtail these phenomena, respectively, is paramount (Al-abri et al., 2009; Al-Abri et al., 2012; Al-Abri, 2011; Benson et al., 2005; Benson and Cole, 2008; Oldenburg and Benson, 2002). The technique of injecting CO_2 into deep saline aquifers and oil and gas reservoirs have the potential for alternative methods for reducing CO_2 emissions (Vilcáez, 2015). Studies (Allen et al., 2017; Bennaceur, 2013; Riis and Halland, 2014; Sanguinito et al., 2018; Sminchak et al., 2017) have shown that deep saline aquifers have the advantage of more storage capacity as a result of different storage mechanisms over oil and gas reservoirs. However, incentives in the form of additional hydrocarbon resources (through Enhanced Oil/Gas Recovery techniques) come from using oil and gas reservoirs as storage sites which will, invariably, offset some of the cost of the sequestration process (Kalra and Wu, 2014). Thus, Enhanced Gas Recovery (EGR) is deemed one of the potential methods for simultaneously storing anthropogenic CO_2 emissions and improving additional natural gas recovery from depleted gas fields, provided that the gas miscibility in situ (mixing) can be reduced. This can be achieved by a better understanding of the mechanisms of displacement and the factors that affect them which will provide vital information for further studies aimed at a wider and robust field scale application and establish the economic viability of the process.

* Corresponding author..
E-mail address: m.k.abba@edu.salford.ac.uk (M.K. Abba).

https://doi.org/10.1016/j.jngse.2018.10.007
Received 11 July 2018; Received in revised form 7 September 2018; Accepted 16 October 2018
Available online 22 October 2018
1875-5100/

The adoption of EGR technique has not been generally well received. This is because of the excessive mixing of the injected carbon dioxide and in-situ natural gas during the flooding process (Al-abri et al., 2009; Honari et al., 2016, 2015; 2013; Hughes et al., 2012; Khan et al., 2013; Oldenburg and Benson, 2002; Shtepani, 2006; Sidiq et al., 2011a; Sim et al., 2008; Zhang et al., 2014). This mixing contaminates the recovered natural gas and reduces its market value by reducing its calorific value and also, incurs additional cost in the sweetening processes (Oldenburg and Benson, 2002; Sim et al. 2008, 2009). This necessitated an in-depth study to unearth ways to minimise this undesirable mixing phenomenon as these two gases are miscible in all ramifications. Mixing can only be minimised if the mechanics and dynamics of the process are understood. To do this, the interplay between different factors that influence the mixing of the injected CO_2 and the nascent CH_4 have to be investigated which will showcase the economic viability of the EGR technology. These factors stem from variations of the physical properties of the fluids, containing reservoir formations and operation conditions such as pressure, temperature, and flowrates.

Many authors (Al-abri et al., 2009; Honari et al., 2016, 2015; 2013; Hughes et al., 2012; Sidiq et al., 2011b; Sidiq and Amin, 2009) have carried out extensive researches on the sensitivity of factors, such as reservoir heterogeneity, pressure, temperature, injection rates, on the mixing between CO_2 and CH_4 to ascertain the influence of these investigated parameters on the gas-gas mixing during EGR. However, limited technical literature are available on the impact of connate water saturation and salinity on CO_2–CH_4 system displacements (Sidiq and Amin, 2009). were the only authors prior to (Honari et al., 2016) to consider connate water saturation when determining the dispersion coefficient of CO_2 in CH_4 in a carbon dioxide-methane systems (Sidiq and Amin, 2009). determined the dispersion coefficient using a new model developed in their work and validated it with experimental data. However, the study was limited to the analysis of the experimental dispersion coefficients to validate the developed model and no comparative analysis was presented between saturated and dry core samples to ascertain the effects of connate water saturation on the displacement process.

A number of literature, as reported by Honari et al. (2016), are available which considered the dispersion in a binary system comprising of different gaseous components (N_2, O_2, H_2O) in the presence of immobile water. In this work, focus is on the experimental investigations in CO_2–CH_4 systems alone. Albeit not exclusively in a CO_2–CH_4 systems, Turta et al. (2007) conducted a series gas-gas displacement tests on Berea cores at a temperature of 70 °C and a pressure of 6.2 MPa using Nitrogen and CO_2 as injection fluids. The tests were conducted both in the presence of connate water and without connate water (dry cores) to investigate the effects of connate water on the recovery efficiency. The tests on consolidated cores showed that for pure nitrogen and pure CO_2, used as the displacing fluids, the recovery was comparable. In the case where a mixture of CO_2 and nitrogen were used to displace the natural gas, it was observed that there were delays in CO_2 breakthrough, associated with a period when only a mixture of methane and nitrogen was produced. This can be attributed to the solubility of CO_2 in connate water which is considerably higher than that of nitrogen. This invariably leads to a higher gas recovery due to a longer resident period, given the fact that a 20% nitrogen contamination in marketable CH_4 tolerable in the produced stream, as opposed to only 2% contamination level for the case of CO_2. They concluded that when using CO_2 as a displacing fluid, recovery was higher in the presence of connate water saturation than in its absence invariably due to the dissolution of CO_2 in the formation brine.

The first ever experimental measurement of dispersion as function of water saturation for supercritical gases in a CH_4–CO_2 system was carried out by Honari et al. (2016). They systematically measured fluid dispersion in various rock cores (sandstones and carbonates), both dry and at irreducible water saturations, at reservoir conditions. They found out that irreducible water increases dispersivity by a factor of up to 7.3. Irreducible water occupied smaller pores creating narrower pores and more tortuous flow paths giving rise to more dispersion/mixing between the injected CO_2 and the in-situ CH_4. Sim et al. (2009a,b) however, inferred that the presence of irreducible water in the reservoir tends to minimise its heterogeneity and as such minimises excessive mixing as shown in their work where they used a sand pack with various degrees of permeability distributions and also a N_2, CH_4, CO_2 binary systems.

These studies, however limited, have touched on the impact of connate water saturation on the displacement efficiency in EGR by CO_2 injection. They have attributed higher dispersion coefficients to the presence of connate water. Conversely, the effect of the salinity/concentration variation of the connate water on the recovery efficiency and or dispersion coefficient was not accounted for. In this paper, the effect of connate water salinity on the dispersion coefficient was investigated experimentally in a consolidated sandstone core sample during CH_4 displacement by supercritical CO_2. Investigating this salinity phenomenon will help reservoir engineers better characterise gas systems for better representation in the adoption of EGR by CO_2 and subsequent sequestration in natural gas reservoirs.

1.1. Theory and concept of enhanced gas recovery

Dispersion is the irreversible mixing that occurs during miscible displacements (Adepoju et al., 2013), it occurs as a result of two simultaneous mechanisms; molecular diffusion and mechanical dispersion (advection) (Perkins and Johnston, 1963). When a miscible fluid displaces another miscible fluid in a porous medium, the displaced fluid tends to mix with the displacing fluid. The efficiency of local displacement in miscible flooding is grossly affected by the mixing taking place within the rock matrix. This mixing is a result of the interaction between these two fluids in contact. A transition or mixing zone develops at the displacement front where the concentration of the displacing fluid decreases from one to zero (Fig. 1). It has been reported (Ekwere, 2007) that several experiments show that the mixing zone propagates longitudinally as displacement process progresses. The macroscopic mixing (dispersion) observed through porous media is used to quantify the mixing taking place (Jha et al., 2013). This can be, to an extent, analysed using empirical evaluation and laboratory experimentation as the concentration of injected CO_2 relative to the in-situ CH_4 in the produced effluent stream.

In order to minimise the cost of producing the recovered natural gas and maximise potential return during enhanced gas recovery, the degree to which injected CO_2 gas mixes with natural gas in situ needs to be well evaluated. Mixing has been found to be controlled by several factors including molecular diffusion/dispersion, pore geometry, turbulence, stagnant fraction of pore space, presence of an immobile fluid, viscous fingering, adsorption/desorption, and gravity segregation (Newberg and Foh, 1988). The viscosity ratio (Eq. (1)) is favourable in the case of supercritical CO_2 displacing CH_4 because CO_2 is more

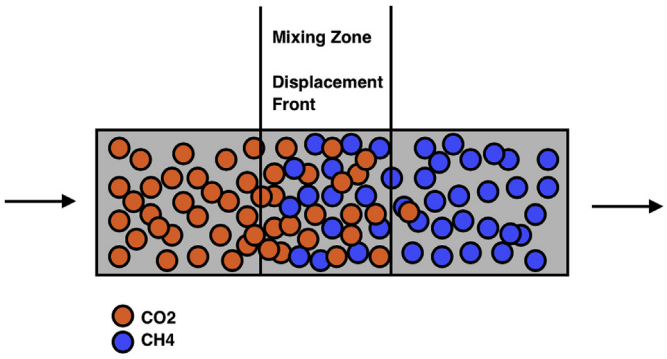

Fig. 1. Schematics of displacement front during CO2 injection displacing CH4.

viscous than CH_4 under reservoir conditions:

$$\frac{\mu CH_4}{\mu CO_2} < 1 \tag{1}$$

Gas transport in porous media occurs widely in numerous applications which include carbons sequestration, oil and gas exploitation, food processing industry etc. The importance of understanding the mechanisms of gas transport in porous media lies in allowing a number of models employed to optimise and evaluate the design and performance of the processes aforementioned.

1.2. Application of gas transport in porous medium in EGR

(Perkins and Johnston, 1963) defined the mixing phenomenon occurring in porous media as a diffusion-like process due to concentration and velocity gradient. The dispersion coefficient denotes the rate of mixing when two miscible fluids come in contact at the displacement front of a flooding process. It depends on the direction of the dispersion flux with respect to the main convective flux. The smallest value of this term occurs perpendicular to the main convective path/flux often called transverse dispersion, and the largest occurs for dispersion in the main convective flux called longitudinal dispersion. Transverse dispersion coefficient, K_t, is more difficult to obtain experimentally and as result, very few data is available in literature besides those of (Perkins and Johnston, 1963).

Newberg and Foh (1988) used a single parameter diffusion-type equation based on the Advection-Dispersion equation (Coats et al., 2009, 1964; Perkins and Johnston, 1963) which was often used to describe the gas transport in porous media to correlate the numerical dispersivities with experimental results and the model is as shown in (Eq. (2)):

$$K_l \frac{\partial^2 C}{\partial x^2} - u\frac{\partial C}{\partial x} = \frac{\partial C}{\partial t} \tag{2}$$

Where, C is the CO_2 concentration at location x at time t, K_L is the coefficient of longitudinal dispersion, and u is the interstitial velocity.

This model was used to generate longitudinal dispersion coefficients and "scale of dispersion" (dispersion coefficient divided by velocity). It also describes the dispersion occurring during the displacement process in EGR.

Invariably (Eq. (2)), may be written in dimensionless form as follows (Mamora and Seo, 2002);

$$\frac{1}{P_e}\frac{\partial^2 C}{\partial x_D^2} - \frac{\partial C}{\partial x_D} = \frac{\partial C}{\partial t_D} \tag{3}$$

Where;

Parameter	Symbol	Expression
Peclet number	P_e	$\frac{uL}{K_l}$
Dimensionless time	t_D	$\frac{tu}{L}$
Dimensionless distance	x_D	$\frac{x}{L}$
Interstitial velociy	u	$\frac{Q}{\pi r^2 \phi}$

L is length of core.
Q is superficial velocity,.
ϕ is porosity.
K_l Longitudinal dispersion .

Since the carbon dioxide injection inlet is at $x = 0$,

then initial condition: $C = 0\ at\ t_D = 0$,
boundary conditions: $C = 1\ at\ x_D = 0,\ C \to 0\ as\ x_D \to \infty$

The solution to (Eq. (3)) maybe shown as follows:

$$C = \frac{1}{2}\left\{erfc\left(\frac{x_D - t_D}{2\sqrt{t_D/P_e}}\right) + e^{P_e x_D} erfc\left(\frac{x_D + t_D}{2\sqrt{t_D/P_e}}\right)\right\} \tag{4}$$

CO_2 concentrations profiles from EGR core flooding experimentation can be compared against those based on analytic solutions of (Eq. (3)) presented in (Eq. (4)) for several values of *Péclet* number, P_e (which is the ratio of advection to dispersion over the experimental length L) from which the corresponding dispersion coefficient can be evaluated.

(Perkins and Johnston, 1963) presented another definition of *Péclet* number termed medium *Péclet* number denoted by, P_{em}, which describes the dominant displacement regime during a dispersion process and expressed in (Eq. (5)) as:

$$P_{em} = \frac{u_m d}{D} \tag{5}$$

Where P_{em} is medium Péclet number, u_m is the mean interstitial velocity (m/s), D is the diffusion coefficient (m^2/s), and d is the characteristic length scale of the porous medium. Generally, at $P_{em} < 0.1$, diffusion dominates the dispersion process and the ratio, is constant and equates to and conversely, at $P_{em} > 10$ advective mixing dominates the dispersion process and the ratio linearly proportional to P_{em}. And in this range of P_{em}, (Coats et al., 2009) correlated dispersion coefficient with diffusion shown in (Eq. (6)):

$$\frac{K_l}{D} = \frac{1}{\tau} + \alpha\frac{u_m^n}{D} \tag{6}$$

Where α is in m and is the dispersivity of the porous medium, n is an exponent. Which is and τ can range from for packed beds and can be as large as 13 for consolidated media as reported by (Honari et al., 2013) and literature therein. The parameter τ can be obtained empirically through several methods, but α and n can only be determined experimentally through core flooding (Hughes et al., 2012).

Furthermore, Takahashi and Iwasaki 1970, as reported by (Hughes et al., 2012) and (Liu et al., 2015), established a correlation between the molecular diffusion coefficient, temperature and pressure. This correlation was used by the authors to obtain accurate diffusivity using (Eq. (7)) at conditions relevant to enhanced gas recovery by CO_2 injection. The correlation is as follows:

$$D = \frac{(-4.3844 \times 10^{-13} p + 8.55440 \times 10^{-11}) T^{1.75}}{p} \tag{7}$$

where D (m^2/s) is the molecular diffusion coefficient of CO_2 in CH_4 at temperature T (K) and pressure p (MPa). In the works of Takahashi and Iwasaki, the diffusion coefficients of CO_2 in CH_4 were measured at 298–348K and pressures of 5–15 MPa in a porous bronze plug which are well within the range of conditions applicable to EGR.

2. Experimental methodology

2.1. Materials used

Pure methane with a purity of 99.995% and research grade carbon dioxide with a purity of 99.999% were supplied by BOC UK a member of the Linde Group. The core sample was obtained from Kocurek Industries USA. The salts employed in this research were supplied by Fisher Scientific UK. The petrophysical properties of the core sample used are shown in Table 1. The porosity was evaluated experimentally using Helium Porosimetry technique.

2.2. Apparatus and procedure

2.2.1. Helium porosimetry

This method facilitates the determination of the grain volume of a core sample which is volume of the rock grains or solids alone. The pore

Table 1
Petrophysical properties of the core sample.

Core sample	Length (mm)	Diameter (mm)	Porosimetry Porosity (%)	Permeability (mD)
Grey Berea	76.27	25.22	20	217

volume was then determined from the difference between the grain volume obtained by this method and the bulk volume which is defined as the volume the sample occupies. The Bulk Volume is determined empirically and analytically by measuring the dimension of the core samples using a high accuracy Vernier caliper and using the cylinder volume determination formulation.

$$Pore\ Volume = Bulk\ Volume - Grain\ Volume \quad (8)$$

Where, $Bulk\ Volume = \frac{\pi d^2}{4} \times L$, and d is the core diameter, and L is core length.

2.2.1.1. Procedure. The Helium gas supply was connected to the gas inlet port of the instrument and was set to 120 psig on the Helium gas bottle regulator. After a leak test, the system grain volume calibration was performed on the Porosimeter (Fig. 2). The matrix cup with reference discs was then connected to the instrument. The sample grain volume measurement was performed, and the obtained results were recorded in the provided application written in excel spreadsheet which evaluated the grain volume of each sample.

2.2.2. Core flooding equipment description

The core flooding equipment used is a branded system by CoreLab Oklahoma, USA. The equipment was modified to carryout gas-gas displacement processes by integrating an Agilent Gas Chromatograph 7890A for effluent analysis depicted in Fig. 3. The core flooding system was rated to 5000 psig confining pressure, 3500 psig pore pressure at room temperature. The inlet pressure into the core sample and outlet pressures on the other side of each core are measured with gauge pressure transducers. An integral part of the system is the SmartFlood software and computer data-acquisition-and-control system hardware which provides on-screen display of all measured values (pressures, temperatures, volumes etc.), automatic logging of test data to a computer data file. The core sample is held within a rubber sleeve inside a Hassler-type core holder by radial confining pressure, which simulates reservoir overburden pressures. The simulated pore pressure was applied through a ISCO model 500D, two-barrel metering pump system with a flow rate range adjustable from 0 to 200 ml/min and a maximum pressure rating of 4000 psig. The overburden (confining) pressure

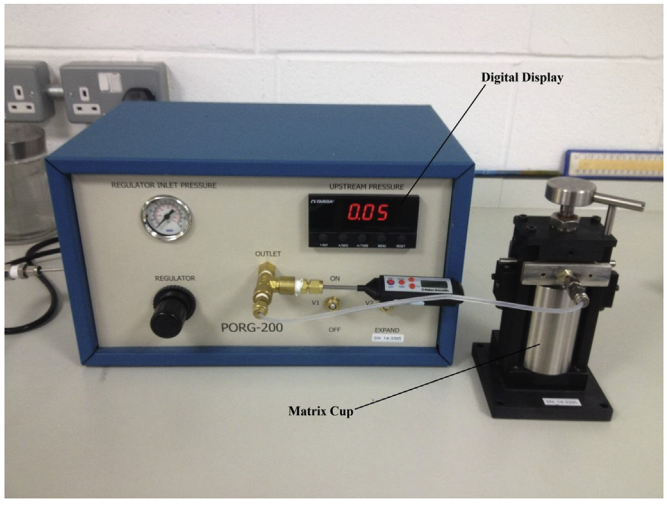

Fig. 2. PORG-200 porosimeter.

pump is a hydraulic pump Model S-216-JN-150 pump, with pressure output of up to 10,000 psig and will provide the desired overburden in the system. The back pressure is regulated with CoreLab dome-loaded type back-pressure regulator which controls the back pressure to a reference pressure supplied to its dome. It is rated for a maximum working pressure of 5000 psig. Floating-piston accumulators are provided as part of the system and are rated for 5000 psig pressure and 350 °F (177 °C) temperature. The accumulators provide for injecting fluids without allowing the fluid to come in contact with the metering pump. 2.5-inch-dial pressure gauges are used to monitor the Overburden Pressure and the BPR Dome Pressure. The pressure range on these gauges is 15,000-psig full scale. Rosemount transducer provided with the system measure differential pressure across the core holder. The effluent flowrate and produced volume was measured by *Bronkhorst* mass flow controllers/meters and records the effluent rates on the logging worksheet of the SmartFlood software. The picture and schematic of the equipment are presented in Figs. 3 and 4.

2.2.2.1. Procedure

2.2.2.1.1. Salt preparation and core sample saturation. The NaCl salt was measured and dissolved in distilled water contained in a round bottom flask with a magnetic stirrer to prepare the desired brine concentrations of 5 and 10 wt%. The core sample was saturated with 10% of its pore volume (determined from Helium porosimetry) with the brine of the concentrations as aforementioned using a vacuum technique. Initial dry runs were first carried out to ascertain repeatability of the set up and method. Then wet runs were performed subsequently, first using distilled water to establish a datum for the salinity variation experiments and then using the prepared concentrations of brine.

2.2.2.1.2. Core flooding. The core sample was wrapped in foil paper to avoid the permeation of the supercritical gases through the sleeve and into the annulus of the core holder. A layer of cling film was first placed between the core sample and the foil paper to prevent the foil paper from sticking to the core sample when subjected to high temperatures and pressures. The core sample was then placed inside the *Viton* sleeve and installed on the distribution plugs of the core holder and secured with clamps on both sides and inserted into the core holder. A heat jacket was placed around the core holder and the temperature ramping was set and the hydraulic pump was initiated to pump the hydraulic oil into the annulus of the core holder to provide the overburden pressure necessary for the experiment in lieu of the simulated reservoir depth pressure. A pressure of 2200 psig was set as the overburden pressure. The simultaneous hydraulic oil pumping and heating was done to avoid high temperature ramping with uncontrolled pressure rise. When the core holder temperature reached 50 °C, the temperature ramping was stopped, and the temperature was kept constant. Hydraulic oil leaks were checked for on both sides of the core holder to ensure that the clamping of the core sample and set up integrities were not compromised.

As a safety precaution, all the valves were shut off. V1 was opened to provide access to the accumulator. D1, depicted in the schematics in Fig. 4, was opened to purge pumps A and B to give room for filling the accumulator A, ACC-A, with the CH_4 gas from the bottle. When there was no increment in the level of the distilled water in the reservoir, D1 was shut off and then V1 was shut off too. The back pressure reference pressure was set to 1300 psig using the N_2 gas bottle. The N_2 gas was used to set the dome pressure of the back pressure regulator as opposed to the hydraulic oil because of the compressibility of the gas which provided a smoother flow of the gas and avoided pressure build-up within the core flooding and the reference pressure was kept constant. V2 was then opened to saturate the system with CH_4. Pumps A&B were engaged to compress the gas in the system to provide the desired system pressure. V2 was then shut off.

The same filling procedure was carried out with accumulator B, ACC-B. V4 was then opened and then the logging commenced and also

Fig. 3. A perspective depiction of the core flooding setup and the gas chromatogragh.

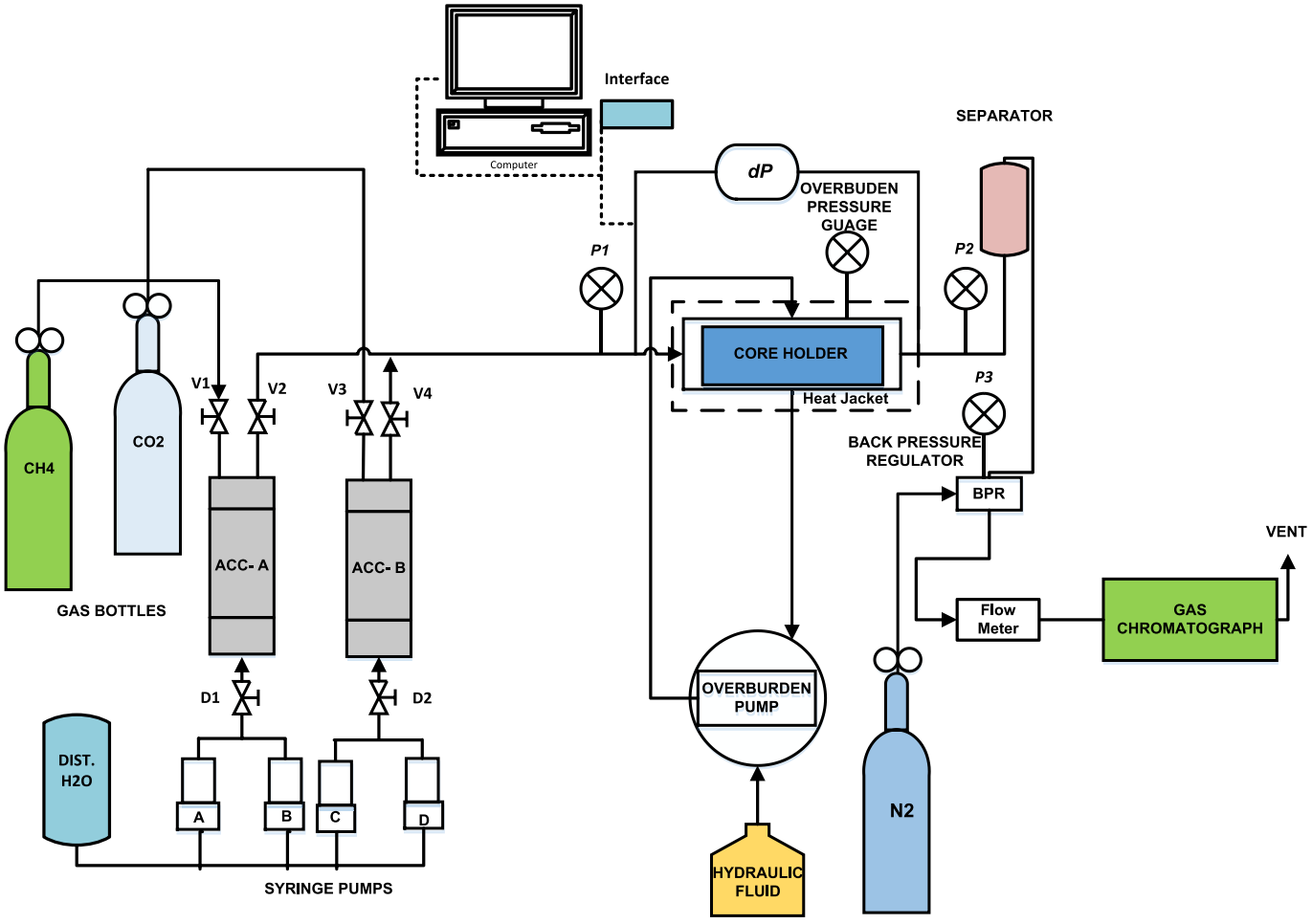

Fig. 4. Schematics of core flooding set up.

the GC sequence as run. The items logged were differential pressure, dP, production rate, each time stamp was recorded which corresponded with the injection times of the GC, whose method sequentially runs for five (5) minutes to sample the effluent every 5 min. The flowrate was measured with the flow meters. The overburden pressure was carefully monitored and was kept more than 500 psig above the pore pressures to avoid the rupturing of the vitton sleeve, given that the pumps deliver a constant flowrate and the pressures rapidly build to maintain the desired flowrate.

Each experimental run came to an end when there were insignificant volumes of CH_4 in the effluent analysis from the GC.

3. Results and discussion

3.1. Optimum injection rate determination

In order to carry out the investigation on the salinity effects on dispersion coefficient, an optimum injection rate for this case was determined. Here, an experimental screening was carried out based on the dispersion coefficient and the CH_4 recovery efficiency to evaluate the optimum injection rate from a range of experimental values – 0.2–0.5 ml/min adopted from literature (Liu et al., 2015). This is to ascertain the best case to evaluate the effects of the connate water salinity during flooding and to minimise other systematic effects emanating from the variation in interstitial velocity within the pore matrix. This systematics, as shown in literature cited within this work, have their various effects on dispersion coefficient and the rock dispersivity.

3.1.1. Dispersion coefficients and dispersivity

A number of displacement runs were carried out to check for consistency and repeatability of the experimental set-up using the same core sample under dry conditions. The evaluated K_L for the test runs are shown in Table 2. When the results became consistent by adjusting the experimental methodology and set-up, the different flowrates were then employed to determine the optimum injection rate from the range of interest. The concentration profiles were used to evaluate the rate of mixing of the injected CO_2 and the nascent CH_4 using (Eq. (3)) as aforementioned and adopting the longitudinal dispersion coefficient K_L as the fitting parameter. The values of the dispersion coefficients for different injection rates are shown in Table 3. The fitted graph of the different injection rates is shown in Fig. 7. The L was adjusted in the regression to provide a better fit as advised by (Hughes et al., 2012) and (Liu et al., 2015) given that the interstitial velocity was held constant as assumed in the 1D advection dispersion equation (Eq. (2)). Least square regression method was employed in the curve fitting technique. As expected, the higher injection rates showed early breakthrough of the CO_2 which is in agreement with the works of (Liu et al., 2015). This also shows that the higher the injection rate the higher the dispersion coefficient as seen in Fig. 5 which showcases the relationship between the two parameters.

Furthermore, the P_{em} was evaluated using (Eq. (5)), in that the characteristic length scale of mixing, d, was evaluated by measuring the mean grain diameter of the core sample using a novel experimental method which will be presented in a subsequent paper. This value was found to be 94 μm. This was then used to determine the dominant mechanism of displacement i.e. the value of the *Peclet* number which was 0.018 meaning that diffusion is the dominant displacement mechanism in the experimental run.

The dispersivity was also evaluated using the relation in (Eq. (6)) where the ratio k/D was plotted against the ratio u/D which is a straight, shown in Fig. 6, and the gradient/slope represented the parameter. The value of the dispersivity was 0.0006m which is well within the range obtained by (Hughes et al., 2012) for consolidated porous media.

Table 2
Dispersion coefficient determination for test runs.

Runs	Q (ml/min)	u (10^{-5} m/s)	Pressure (psig)	Temperature (°C)	K_L (10^{-8} m^2/s)
Run 1	0.25	3.45	1300	50	1.989
Run 2	0.25	3.45	1300	50	4.125
Run 3	0.25	3.45	1300	50	8.732
Run 4	0.25	3.45	1300	50	2.681
Run 5	0.25	3.45	1300	50	2.849
Run 6	0.25	3.45	1300	50	2.206
Run 7	0.25	3.45	1300	50	2.848
Run 8	0.25	3.45	1300	50	2.452

3.1.2. Optimum CH_4 recovery efficiency

To determine the percentage recovery of the CH_4, the original gas in place OGIP was determined using (Eq. (9)). The porosity obtained from the He porosimetry, the Gas formation volume factor was calculated at the experimental conditions with the compressibility factor, Z, obtained numerically from the models in works of (Shabani and Vilcáez, 2017; Ziabakhsh-Ganji and Kooi, 2012) which provided a better presentation of the parameter.

$$G = \frac{v_b \phi (1 - S_w)}{B_g} \tag{9}$$

The value of the OGIP was then used to calculate the CH_4 percentage recovery using the production rates obtained from the mass flow meters of the core flooding set-up. CH_4 production recovery, expressed as pore volumes produced, was evaluated and plotted as a function of time which as shown in Fig. 8.

Fig. 8 is a representation of the results of the CH_4 production recovery efficiency obtained from the core flooding experiments using different injection rates at the same reservoir conditions. Each run has a characteristic peculiarity and trend. For the experimental run at 0.2 ml/min, the recovery was substantial but the resident time for the displacement was longer and hence a stream of CH_4 laced or contaminated by the CO_2 was recovered. In that, there was substantial mixing between the displaced and displacing gases given the nature of the miscibility between them albeit having lower dispersion coefficient. This is not conceivably an economic derivative as more CH_4 will be produced which will be grossly contaminated by the injected CO_2 thereby undermining the sequestration idea.

Consequently, the experimental run at 0.3 ml/min showcases a different scenario with the highest recovery trend in all the experimental runs. There was a substantial CH_4 recovery and good sweep efficiency compared to the runs of 0.4 ml/min and 0.5 ml/min which show a very poor trend in terms of CH_4 recovery and sweep efficiency as a result of higher interstitial velocity. High interstitial velocities tend to increase the turbulence of the flow profile and agitate the molecules of the gas species which in turn facilitates the interaction between the displacing and displaced fluids.

With the results from the dispersion coefficient determination and CH_4 recovery efficiency, it is apparent that the best and optimum injection rate for CO_2 for this experiment is the 0.3 ml/min. Thus, this flow rate will be adopted in the main experiment to investigate the effect of connate water salinity on dispersion.

3.2. Connate water salinity investigation

Having determined the optimum CO_2 injection rate, the next step was to investigate the effect of connate water salinity on dispersion coefficient using the obtained injection rate. The connate water saturation was set to 10% to establish an immobile phase at the operating conditions based on the size and pore geometry of the core sample. This was done by saturating the core sample with 10% of its pore volume

Table 3
Dispersion coefficient determination for different injection rates.

Q (ml/min)	Pressure (psig)	Temperature (°C)	u (10^{-5} m/s)	K_L (10^{-8} m^2/s)	D (10^{-8} m^2/s)
0.2	1300	50	3.31	1.41	22.56
0.3	1300	50	5.01	2.69	22.56
0.4	1300	50	6.66	3.01	22.56
0.5	1300	50	8.33	3.85	22.56

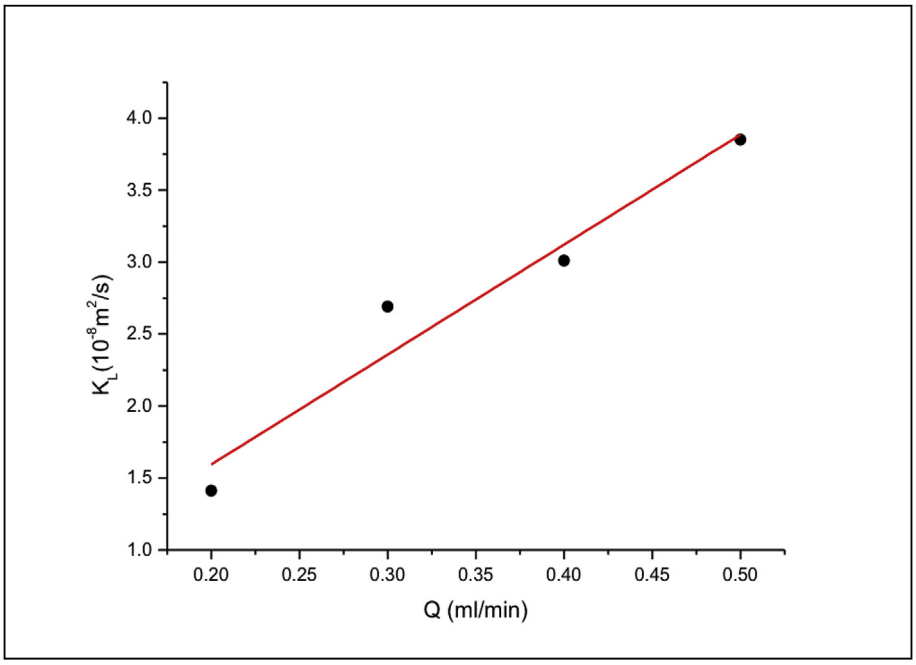

Fig. 5. Variation of Dispersion coefficient with injection rate.

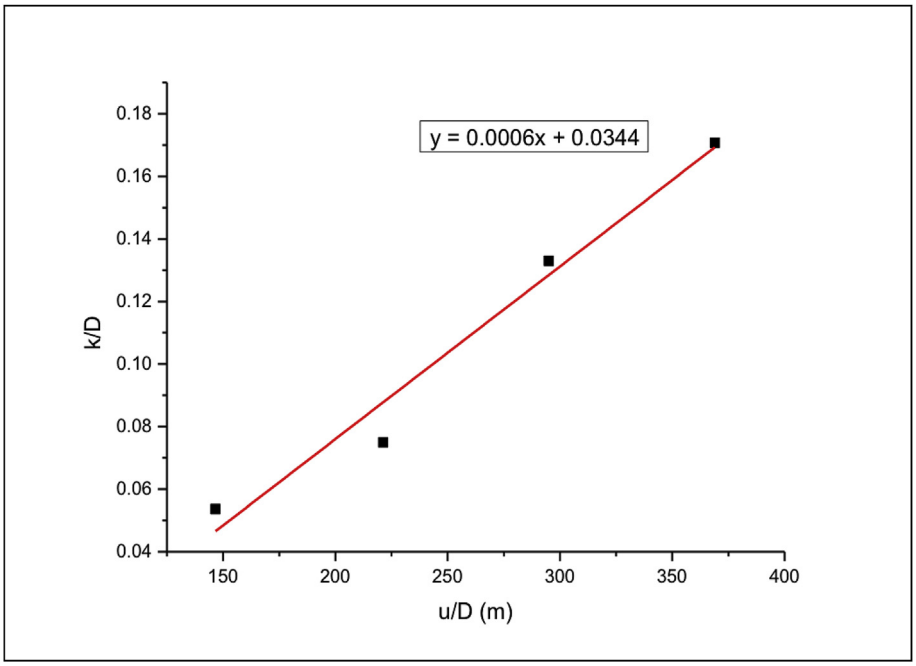

Fig. 6. Dispersity of the core sample at test conditions.

with distilled water, brine (5 wt%), and brine (10 wt%) under vacuum for effective distribution throughout the pore matrix of the core sample.

The dispersion coefficient of each saturation and salinity will be highlighted to evaluate the effect of the both parameters on the mixing during EGR.

3.2.1. Dispersion coefficient measurement

Table 4 shows the results obtained from curve fitting the

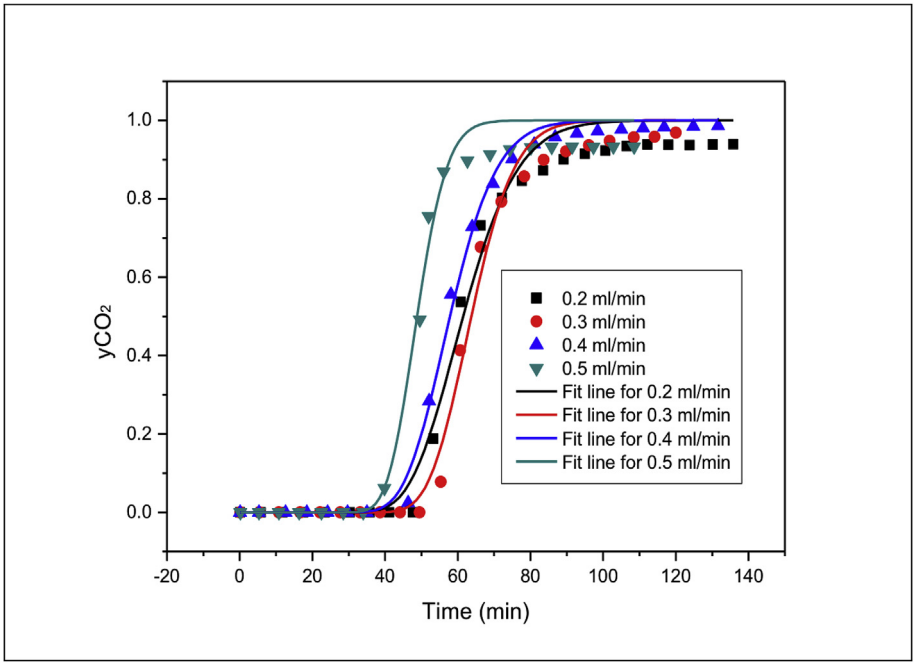

Fig. 7. Fitted concentration profiles of different experimental runs.

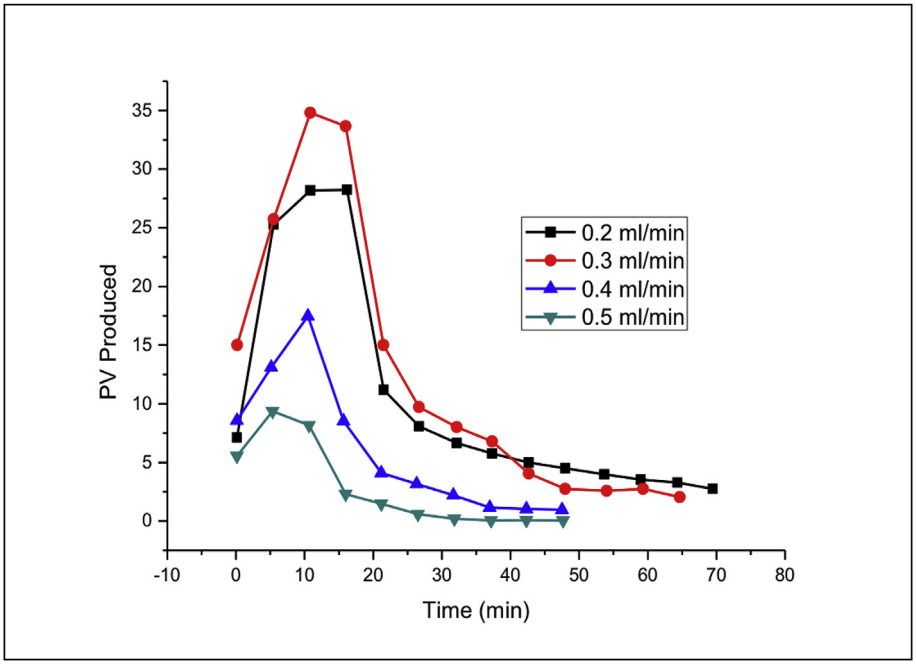

Fig. 8. CH_4 recovery as a function of time.

Table 4
Dispersion coefficient as a function of salinity.

Run	S_{wi} (%)	Salinity (wt %)	Pressure (psig)	Temperature (°C)	K_L (10^{-8} m^2/s)
1	10	10	1300	50	0.44
2	10	5	1300	50	0.59
3	10	0	1300	50	3.61
4	0	0	1300	50	2.82

experimental data obtained from core flooding at different salinities but at the same operation conditions.

The results are consistent with the finding of (Abba et al., 2017) who carried out the investigation at a temperature of 40 °C and a pressure of 1300 psig. They explained the trend observed was as a result of reduction in the tortuous flow paths of the porous medium with connate water inclusion in the experimental run. However, when distilled water was used, the distribution of the water in the pore matrix did not completely seal off smaller pores but instead reduced the pore throats resulting in narrower flow paths and hence higher interstitial velocities. Here, the dispersion coefficient was highest, which was attributed that the low density of the connate water, compared to the brines, was responsible for higher dispersion coefficient observed.

The fitted curves of the concentration profiles are shown in Fig. 9. Early breakthrough of CO_2 was apparent in the runs with saturations of

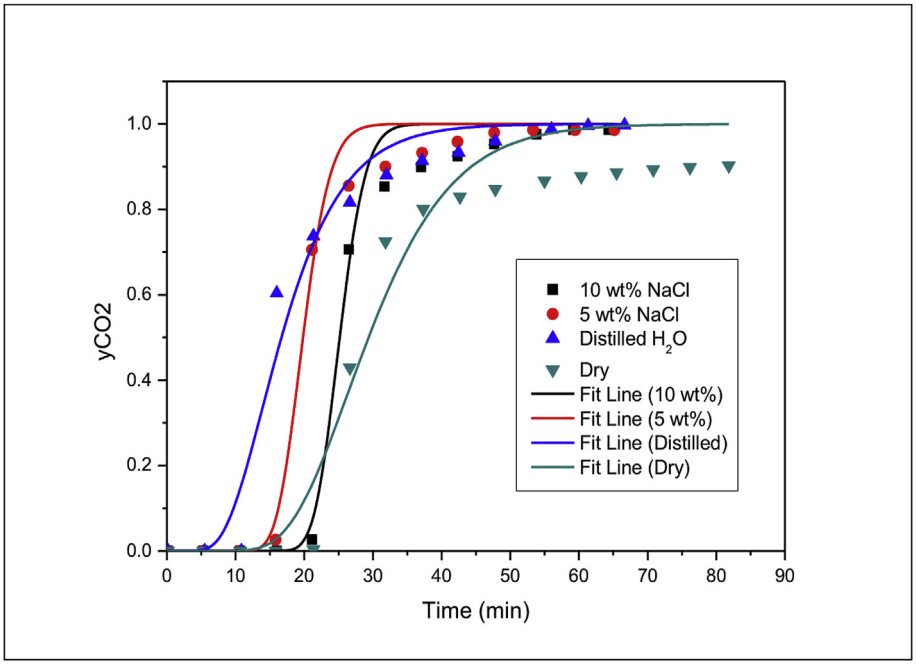

Fig. 9. Concentration profiles of different variants of salinities and air at test conditions.

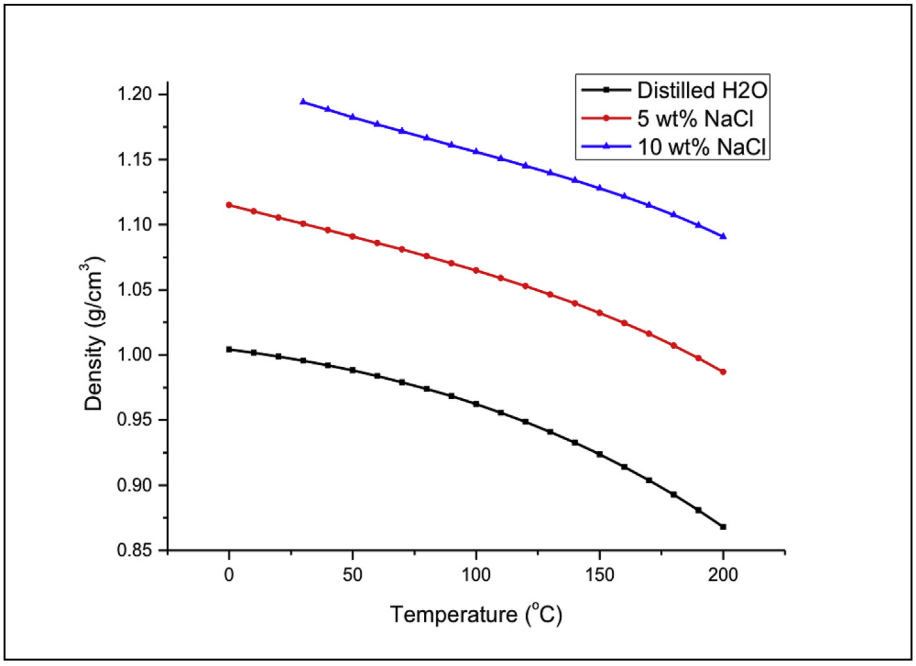

Fig. 10. Connate water densities as functions of temperature at 1400 psig (Generated from PVTsim 20).

Table 5
Brine concentrations with corresponding densities.

Salinity (wt%)	Temperature (°C)	Pressure (psig)	Density (g/cm^3)
10	50	1300	1.18245
5	50	1300	1.09095
0	50	1300	0.98796

10% by volumes, given that the pore volume of the core sample was reduced by 10% due to the inclusion of connate water.

There was meagre fitting of the analytical solution to the experimental data at the tail end of the concentration profiles and this was as a result of the entry and exit effects of the displacing supercritical CO_2 which was pointed out by (Honari et al., 2013; Hughes et al., 2012) and reiterated by (Liu et al., 2015). Details of this tailing effect are presented in (Liu et al., 2015).

The densities of the different connate water salinities were simulated and shown in Fig. 10 using PVTsim 20. This was carried out to highlight the interplay between the formation water salinities and the dispersion coefficient. This relationship between the connate water salinity and the dispersion coefficient is first shown in this body of work to the knowledge of this research.

From the simulation results, the densities were extracted at the desired conditions and tabulated below in Table 5.

Properties tabulated in Table 6 clearly show the observed

Table 6
Fluid densities with corresponding dispersion coefficients.

Run	Salinity (wt%)	Density (g/cm^3)	K_L (10^{-8} m^2/s)
1	10	1.18245	0.44
2	5	1.09095	0.59
3	0	0.98796	3.61

relationship between connate water densities and the longitudinal dispersion coefficients. The postulate that as the density of the connate water in the pore spaces of the core sample increases, the dispersion coefficient decreases is shown graphically in Fig. 11:

Albeit the good fit of the data in the graph, the standard error in the fit-line was within 1% of the average of the experimental data. The graph is mainly for representation and not aimed at describing a model to relate these two properties as there is no data, to the knowledge of this research, found in literature to back up this finding. However, this is a new data in the description of the CO_2 dispersion in CH_4 in consolidated porous media at conditions relevant to EGR.

The time it will take for the injected CO_2 to pass through the core sample will grossly be reduced since the tortuosity is reduced by the inclusion of connate in the core sample given the homogeneous nature of the core sample. This can explain what was observed in the experimental runs with higher density connate water as shown in Fig. 12. The pressure drop across the core sample during the run with 10%wt connate water was considerably higher in comparison with the other concentrations. Due to the high density of 10 wt% connate water (1.18245 g/cm^3), the capillary forces within the narrower pores in the core sample were overcome and the connate water occupied those pores thereby sealing some of the flow paths within the pore network. This reduces the flow channels, significantly, through which the injected CO_2 will flow to displace the nascent CH_4 which will eventually lead to higher pressure build-up in the core sample as the CO_2 transverses the now less tortuous and more constricted core matrix. With this higher pressure drop (ΔP), a lower permeability is evident according to Darcy relationship between permeability (k) and ΔP which states that permeability is inversely proportional to the differential pressure across a core sample as shown in (Eq. (10)). The injected CO_2 permeability decreased with increase in the density of the connate water.

$$k = \frac{q\mu L}{A\Delta P} \tag{10}$$

Where k is the permeability (md), q is flowrate (cm^3/s), μ is fluid viscosity (cp), A is cross sectional area of core (cm^2), and ΔP is differential pressure across the core sample (atm).

However, the experimental run with distilled water showed a higher differential pressure, invariably lower permeability, compared to that of the 5 wt%. This can be as result of the reason given by (Abba et al., 2017) that due to the lower density of the distilled water compared to that of the brine, the capillary forces within the pore matrix were not overcome by the density of the distilled water. Therefore, the distilled water did not entirely block or seal off the narrower flow paths, as in the case of the 10 wt% connate water, of the core sample as suggested by (Honari et al., 2016). Instead, it made it narrower and that decreased the permeability of the core sample and this phenomenon also explains the high dispersion coefficient observed with the Distilled water experimental run as shown in Table 4. This clearly shows the influence of connate water salinity on the dispersion coefficient, invariably the mixing of the gases during EGR. For 5 wt % brine, the low ΔP and high permeability translated to the sealing off narrower and smaller pore spaces, some of whose capillary forces superseded the density of the brine in question. Therefore, more flow channels were available for flow without impending restrictions as seen in the case of the 10 wt% brine experiment. Thus, the flow behaviour was close to that of the dry run were there was no inclusion of connate water. In higher salinity connate water environment, a lower mixing is expected because of the more homogenous flow paths as discussed earlier. This finding will be vital in the accurate depiction of EGR during simulation studies for field scale applications of the technique.

4. Conclusion

The optimum flow conditions for the connate water salinity effect on dispersion coefficient were successfully evaluated through systematic and comparative experimental. These were based on the CH_4 recovery and favourable dispersion coefficient of each investigated injection rate. Optimum flow conditions obtained were used to carry out the connate water salinity investigation. From the results, it can be inferred that an increase in the brine density, as a result of increasing its

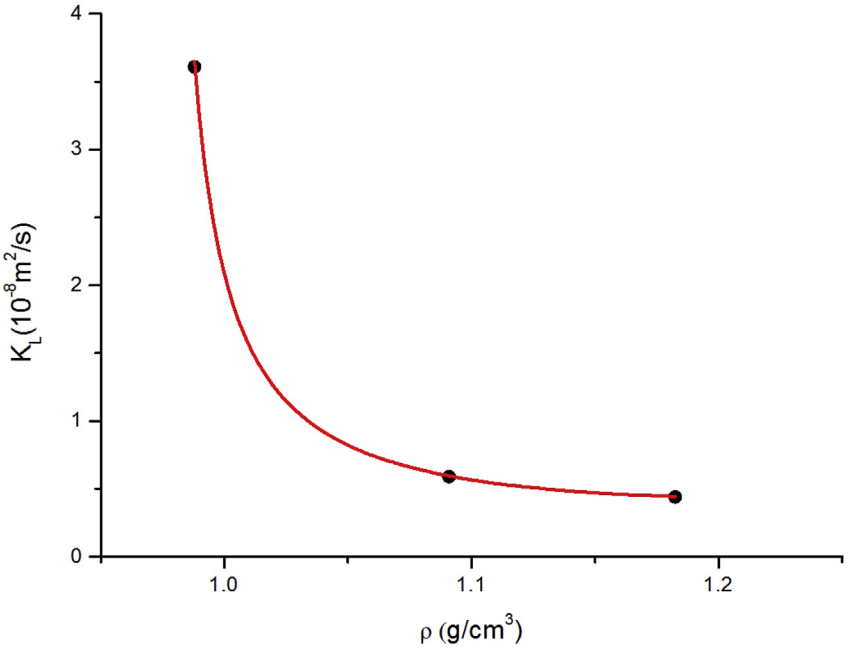

Fig. 11. Dispersion Coefficient as a function of connate water density.

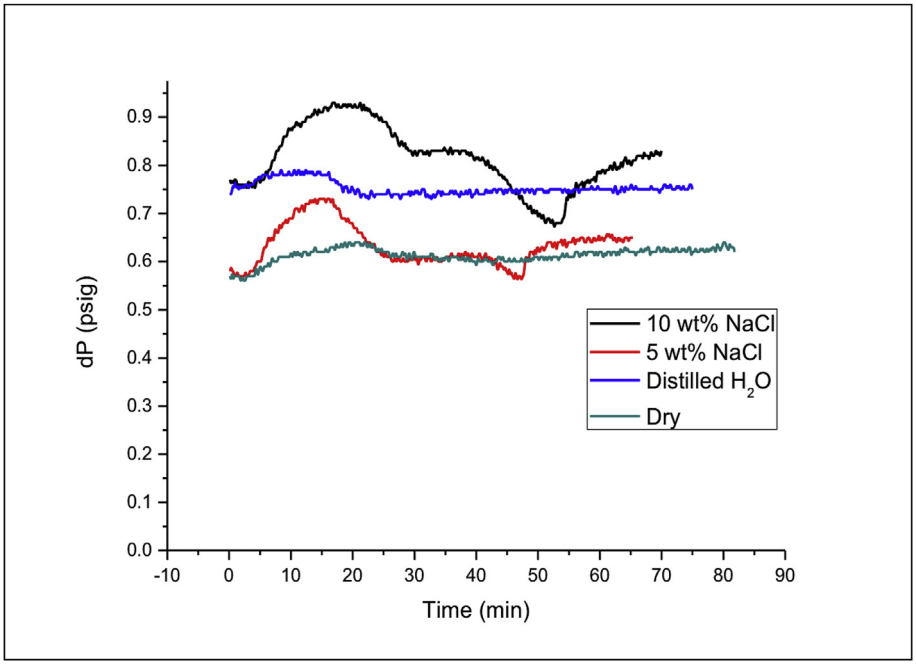

Fig. 12. Differential pressure of the experimental runs as a function of time.

concentration, increased the dispersion coefficient. The density of the connate water plays a significant role in the flow behaviour of the injected CO_2 in a way that it dictates the flow channels and matrix of the reservoir rock through which the displacement process develops. As seen with the experimental run using the 10 wt% brine with a density of 1.18245 g/cm^3, the dispersion coefficient was 8 times less than that of the distilled water with density of 0.98796 g/cm^3. This will have a major effect on the contamination of the produced natural gas from the reservoir through EGR. Thus, inclusion of connate water salinity in simulation studies for EGR field application could provide significant understanding of realistic displacement process in sandstones reservoirs.

Acknowledgement

The authors wish to gratefully acknowledge Petroleum Technology Development Fund (PTDF) Nigeria for the studentship. The support from the Spray Research Group (SRG) will not go unnoticed and also the consultation and input of Petroleum Research Group (PTRG) University of Salford UK.

Nomenclature

B_g	Gas formation volume factor, cm^3/scm^3
C	CO_2 mole fraction
D	Diffusion coefficient, m^2/s
d	Characteristic length scale, m
G	Original Gas in place, cm^3
k	Permeability, md
K_L	Longitudinal dispersion, m^2/s
L	Core sample length, mm
L_{exp}	Experimental length, m
μ	Viscosity, cP
P	Pressure, psig
P_e	Peclet number
P_{em}	Medium Peclet number
Q	Flowrate, ml/min
R	Radius of core sample, mm
S_w	Connate water saturation
T	Temperature, °C
t	Time, min
t_D	Dimensionless time
u	interstitial velocity, m/s
x	Distance from the upstream of the core face, m
x_D	Dimensionless distance
ϕ	Core porosity

References

Abba, M.K., Abbas, A.J., Nasr, G.G., 2017. Enhanced gas recovery by CO2 injection and sequestration: effect of connate water salinity on displacement efficiency. SPE Abu Dhabi Int. Pet. Exhib. Conf. https://doi.org/10.2118/188930-MS.

Adepoju, O.O., Lake, L.W., Johns, R.T., Energy, E.M.S., 2013. SPE 166390 Anisotropic Dispersion and Upscaling for Miscible Displacement. pp. 421–432.

Al-abri, A., Sidiq, H., Amin, R., 2009. Enhanced natural gas and condensate recovery by injection of pure SCCO2, pure CH4 and their Mixture: experimental investigation. In: SPE Annu. Tech. Conf. Exhib. New Orleans, Lousiana, USA, 4-7 Oct. 1–13.

Al-Abri, A., Sidiq, H., Amin, R., 2012. Mobility ratio, relative permeability and sweep efficiency of supercritical CO2 and methane injection to enhance natural gas and condensate recovery: coreflooding experimentation. J. Nat. Gas Sci. Eng. 9, 166–171. https://doi.org/10.1016/j.jngse.2012.05.011.

Al-Abri, A.S., 2011. Enhanced Gas Condensate Recovery by CO 2 Injection.

Allen, R., Nilsen, H.M., Andersen, O., Lie, K.A., 2017. Categorization of Norwegian continental shelf formations in terms of geological CO2Storage potentials. Energy Procedia 114, 4583–4594. https://doi.org/10.1016/j.egypro.2017.03.1579.

Bennaceur, K., 2013. CO2Capture and sequestration. Futur. Energy Improv. Sustain. Clean Options our Planet 583–611. https://doi.org/10.1016/B978-0-08-099424-6.00026-0.

Benson, S., Cook, P., Anderson, J., Bachu, S., Nimir, H.B., Basu, B., Bradshaw, J., Deguchi, G., 2005. Underground Geological Storage. Ipcc, pp. 195–276.

Benson, S.M., Cole, D.R., 2008. CO2 sequestration in deep sedimentary formations. Elements 4, 325–331. https://doi.org/10.2113/gselements.4.5.325.

Coats, K.H., Smith, B.D., van Genuchten, M.T., Wierenga, P.J., 1964. Dead-end pore volume and dispersion in porous media. Soil Sci. Soc. Am. J. 4, 73–84. https://doi.org/10.2118/647-PA.

Coats, K.H., Whitson, C.H., Thomas, K., 2009. Modeling conformance as dispersion. SPE Reservoir Eval. Eng. 12, 33–47. https://doi.org/10.2118/90390-PA.

Ekwere, P.J., 2007. Petrophysics 1049.

Honari, A., Bijeljic, B., Johns, M.L., May, E.F., 2015. Enhanced gas recovery with {CO2} sequestration: the effect of medium heterogeneity on the dispersion of supercritical CO2–CH4. Int. J. Greenh. Gas Control 39, 39–50. https://doi.org/10.1016/j.ijggc.2015.04.014.

Honari, A., Hughes, T.J., Fridjonsson, E.O., Johns, M.L., May, E.F., 2013. Dispersion of supercritical CO2 and CH4 in consolidated porous media for enhanced gas recovery simulations. Int. J. Greenh. Gas Control 19, 234–242. https://doi.org/10.1016/j.ijggc.2013.08.016.

Honari, A., Zecca, M., Vogt, S.J., Iglauer, S., Bijeljic, B., Johns, M.L., May, E.F., 2016. The

impact of residual water on CH4-CO2 dispersion in consolidated rock cores. Int. J. Greenh. Gas Control 50, 100–111. https://doi.org/10.1016/j.ijggc.2016.04.004.
Hughes, T.J., Honari, A., Graham, B.F., Chauhan, A.S., Johns, M.L., May, E.F., 2012. CO2 sequestration for enhanced gas recovery: new measurements of supercritical CO2–CH4 dispersion in porous media and a review of recent research. Int. J. Greenh. Gas Control 9, 457–468. https://doi.org/10.1016/j.ijggc.2012.05.011.
Jha, R.K., Bryant, S.L., Lake, L.W., John, A., 2013. Investigation of pore-scale (local) mixing. SPE/DOE Symp. Improv. Oil Recover. https://doi.org/10.2118/99782-MS.
Kalra, S., Wu, X., 2014. CO2 injection for enhanced gas recovery. SPE West. North Am. Rocky Mt 16–18.
Khan, C., Amin, R., Madden, G., 2013. Carbon dioxide injection for enhanced gas recovery and storage (reservoir simulation). Egypt. J. Pet. 22, 225–240. https://doi.org/10.1016/j.ejpe.2013.06.002.
Liu, S., Zhang, Y., Xing, W., Jian, W., Liu, Z., Li, T., Song, Y., 2015. Laboratory experiment of CO2-CH4 displacement and dispersion in sandpacks in enhanced gas recovery. J. Nat. Gas Sci. Eng. 26, 1585–1594. https://doi.org/10.1016/j.jngse.2015.04.021.
Mamora, D.D., Seo, J.G., 2002. Enhanced recovery by carbon dioxide sequestration in depleted gas reservoirs. SPE Annu. Tech. Conf. Exhib. 1–9.
Newberg, M., Foh, S., 1988. Measurement of longitudinal dispersion coefficients for gas flowing through porous media. SPE 5–9.
Oldenburg, C.M., Benson, S.M., 2002. CO2 injection for enhanced gas production and carbon sequestration. SPE Int. Pet. Conf. Exhib. Mex. https://doi.org/10.2118/74367-MS.
Perkins, T., Johnston, O., 1963. A review of diffusion and dispersion in porous media. Soc. Petrol. Eng. J. 3, 70–84. https://doi.org/10.2118/480-PA.
Riis, F., Halland, E., 2014. CO2 storage atlas of the Norwegian Continental shelf: methods used to evaluate capacity and maturity of the CO2 storage potential. Energy Procedia 63, 5258–5265. https://doi.org/10.1016/j.egypro.2014.11.557.
Sanguinito, S., Goodman, A.L., Sams, J.I., 2018. CO2-SCREEN tool: application to the oriskany sandstone to estimate prospective CO2storage resource. Int. J. Greenh. Gas Control 75, 180–188. https://doi.org/10.1016/j.ijggc.2018.05.022.
Shabani, B., Vilcáez, J., 2017. Prediction of CO2-CH4-H2S-N2gas mixtures solubility in brine using a non-iterative fugacity-activity model relevant to CO2-MEOR. J. Petrol. Sci. Eng. 150, 162–179. https://doi.org/10.1016/j.petrol.2016.12.012.
Shtepani, E., 2006. CO2 sequestration in depleted gas/condensate reservoirs. In: Proc. - SPE Annu. Tech. Conf. Exhib..
Sidiq, H., Amin, R., 2009. Mathematical model for calculating the dispersion coefficient of super critical CO2 from the results of laboratory experiments on enhanced gas recovery. J. Nat. Gas Sci. Eng. 1, 177–182. https://doi.org/10.1016/j.jngse.2009.11.001.
Sidiq, H., Amin, R., der Steen, E. Van, Kennaird, T., 2011a. Super critical CO2-methane relative permeability investigation. J. Petrol. Sci. Eng. 78, 654–663. https://doi.org/10.1016/j.petrol.2011.08.018.
Sidiq, H., Amin, R., der Steen, E. Van, Kennaird, T., 2011b. Super critical CO2-methane relative permeability investigation. J. Petrol. Sci. Eng. 78, 654–663. https://doi.org/10.1016/j.petrol.2011.08.018.
Sim, S., Turta, A.T., Singhal, A., Hawkins, B.F., 2009a. Enhanced gas recovery: effect of reservoir heterogeneity on gas-gas displacement. Candian Int. Pet. Conf. 1–14. https://doi.org/10.2118/2009-023.
Sim, S., Turta, A.T., Singhal, A.K., Hawkins, B.F., 2009b. Enhanced gas recovery: factors affecting gas-gas displacement efficiency. J. Can. Pet. Technol. 48, 49–55. https://doi.org/10.2118/09-08-49.
Sim, S.S.K., Brunelle, P., Canada, Q., Systems, F., Turta, A.T., Singhal, A.K., 2008. SPE 113468 enhanced gas recovery and CO 2 sequestration by injection of exhaust gases from combustion of bitumen. Changes 1–10.
Sminchak, J.R., Babarinde, O., Gupta, N., 2017. Integrated analysis of geomechanical factors for geologic CO2Storage in the midwestern United States. Energy Procedia 114, 3267–3272. https://doi.org/10.1016/j.egypro.2017.03.1458.
Turta, A.T., Sim, S.S.K., Singhal, A.K., Hawkins, B.F., 2007. Basic Investigations on Enhanced Gas Recovery by Gas-Gas Displacement.
Vilcáez, J., 2015. Numerical modeling and simulation of microbial methanogenesis in geological CO2storage sites. J. Petrol. Sci. Eng. 135, 583–595. https://doi.org/10.1016/j.petrol.2015.10.015.
Zhang, Y., Liu, S., Song, Y., Zhao, J., Tang, L., Xing, W., Jian, W., Liu, Z., Zhan, Y., 2014. Experimental investigation of CO2-CH4 displacement and dispersion in sand pack for enhanced gas recovery. Energy Procedia 61, 393–397. https://doi.org/10.1016/j.egypro.2014.11.1133.
Ziabakhsh-Ganji, Z., Kooi, H., 2012. An Equation of State for thermodynamic equilibrium of gas mixtures and brines to allow simulation of the effects of impurities in subsurface CO2storage. Int. J. Greenh. Gas Control 11, 21–34. https://doi.org/10.1016/j.ijggc.2012.07.025.